

Octagonal tilings with three prototiles

April Lynne D. Say-awen¹ and Sam Coates²

¹*Mathematics and Statistics Department, De La Salle University, Malate, Manila, 1004, Philippines**

²*Surface Science Research Centre, Department of Physics,
University of Liverpool, Liverpool L69 3BX, United Kingdom*

(Dated: February 7, 2025)

Motivated by theoretically and experimentally observed structural phases with octagonal symmetry, we introduce a family of octagonal tilings which are composed of three prototiles. We define our tilings with respect to two non-negative integers, m and n , so that the inflation factor of a given tiling is $\delta_{(m,n)} = m + n(1 + \sqrt{2})$. As such, we show that our family consists of an infinite series of tilings which can be delineated into separate ‘cases’ which are determined by the relationship between m and n . Similarly, we present the primitive substitution rules or decomposition of our prototiles, along with the statistical properties of each case, demonstrating their dependence on these integers.

1 Introduction and motivation

Aperiodic tilings are well-studied across the physical sciences: they can be analysed through their structural properties [1–6], explored via physical models and simulations [7–15], and employed as tools to enhance our understanding of quasicrystalline materials [16–18]. This latter point has been key to the rigorous structural understanding of quasicrystalline phases across different states of matter which, broadly speaking, can be delineated by their rotational symmetries. For instance, stable intermetallic alloy quasicrystals exhibit either icosahedral or decagonal symmetry, such that their high symmetry planes can be mapped using 2-, 3-, 5-fold (icosahedral), or 2-, 10-fold (decagonal) tilings. Either predicted or observed, the non-alloy quasicrystalline phases (liquid, colloidal, oxide etc. [19–24]) are, in the vast majority [25], found to exhibit octagonal or dodecagonal rotational symmetries. Typically, the aperiodic tilings used to describe these octagonal and dodecagonal structures are composed of triangles and squares, and can be random or highly ordered. While the building blocks of these tilings are quite simplistic, the number of possible periodic or aperiodic structural variations is staggering [26].

Recent theoretical work on the self-assembly of hard spheres of two radii on a flat plane showed a rich structural phase diagram, which included octagonal and dodecagonal phases [19]. Indeed, a physical representation of one such phase has also been realised [20]. In the theoretical work, phase selection can be controlled by the size ratio of the spheres (small:large, labelled q) and the fraction of small spheres, x_S . Here, the quasicrystalline phases were characterized using random aperiodic tiling models built of triangles and squares. For the dodecagonal cases, the constituent tiles were a square and an equilateral triangle, congruent with the building blocks of the square-triangle Schlottmann tiling [27, 28]. For the octagonal cases, the constituent tiles are a small square, a large square, and an isosceles triangle, which as yet, do not belong to a tiling family. As the authors state: ‘our results exhibit completely new types of aperiodic octagonal tilings, which, to the best of our knowledge, have not yet been described in the literature.’ [19].

The motivation for our work comes directly from addressing this statement, in which we wish to introduce a new family of octagonal tilings which are composed of three prototiles. The structure of our paper is as follows: first, we introduce the basic ingredients and nomenclature needed to describe our tilings, using the Ammann-Beenker tiling as an example. Then, we demonstrate how

* april.say-awen@dlsu.edu.ph

to construct the substitution rules of our family, before discussing tiling properties. Finally, we show some tiling variants and edge cases, before comparing our family to existing tilings in the literature.

2 Basics

For any polygon P , we denote its interior by $\text{int}(P)$ and its area by $A(P)$. Given a collection \mathcal{A} of polygons, we define the *support* of \mathcal{A} , denoted by $\text{supp}(\mathcal{A})$, as the union of the polygons in \mathcal{A} .

A *tiling* in the plane is a collection \mathcal{T} of tiles such that $\text{supp}(\mathcal{T}) = \mathbb{R}^2$ and the intersection of the interiors of two distinct tiles T and T' is empty (i.e., $\text{int}T \cap \text{int}T' = \emptyset$ if $T \neq T'$). (In this work, tiles are polygons.) A prototile set \mathcal{F} of a tiling \mathcal{T} is a set of non-congruent tiles, called prototiles, such that each tile in \mathcal{T} is congruent to a tile in \mathcal{F} . The prototiles can be thought of as the building blocks of the tiling \mathcal{T} . Any finite subset of a tiling is called a *patch* of \mathcal{T} . A powerful method for generating tilings - particularly aperiodic ones - is the use of substitution rules, which generally fall into two types: self-similar and pseudo substitution rules.

A self-similar substitution rule can be viewed as “inflate-and-subdivide” rule. The basic idea begins with a finite set of prototiles T_1, T_2, \dots, T_m and an inflation factor $\lambda > 1$. A substitution rule σ maps each T_i to a set $\sigma(T_i)$ consisting of tiles, each congruent to a prototile, such that $\text{supp}(\sigma(T_i)) = \lambda T_i$, and the intersection of the interiors of any two distinct tiles in $\sigma(T_i)$ is empty. One can iterate the substitution on a prototile or patch contained by $\sigma(T_i)$. Specifically, the patch $\sigma^k(T_i)$, which results from iterating the substitution on T_i k times is called the *k -order supertile* of T_i .

The action of a pseudo substitution rule is similar to that of a self-similar substitution rule, except that some tiles in $\sigma(T_i)$ extend beyond λT_i in a consistent manner. Specifically, if two distinct tiles have overlapping interiors in a k -order supertile for $k \geq 2$, they must overlap entirely. In this work, we focus on the case where $\text{supp}(\sigma(T_i)) \supset \lambda T_i$, with the edges of λT_i bisecting any tiles not fully contained within λT_i .

Any patch contained by a supertile of σ is called a *legal patch* of σ . A tiling \mathcal{T} is a *substitution tiling* corresponding to σ if every patch of \mathcal{T} is a legal patch of σ .

One of the classic examples of a substitution tiling is the Ammann-Beenker (AB) tiling. The first known substitution rule associated to the AB tiling [1, 29] is shown in Figure 1a, which is a pseudo substitution rule. The inflation factor is given by $\mu = 1 + \sqrt{2}$. Note that the substitution rule breaks the symmetry of T_2 , necessitating the decoration of T_2 and all its copies to indicate their orientations. Without these decorations, the k -order supertile cannot be defined for all $k \geq 2$. Figure 2 shows the 2-order supertile of T_1 , highlighting overlapping tiles. The AB tiling can also be obtained using the self-similar substitution rule [30] shown in Figure 1b. For any supertile of this substitution rule, the triangles pair up to form squares congruent to T_2 .

A common method to obtain a substitution tiling using a substitution rule σ is by iterating σ on a legal patch. Specifically, to construct a tiling with n -fold rotational symmetry, start with a legal patch \mathcal{P} invariant under n -fold rotation, with its center at the origin. Iterating σ on \mathcal{P} , we seek a positive integer k such that $\mathcal{P} \subset \sigma^k(\mathcal{P})$. If such a k exists, the nested sequence $\mathcal{P} \subset \sigma^k(\mathcal{P}) \subset \sigma^{2k}(\mathcal{P}) \subset \sigma^{3k}(\mathcal{P}) \subset \dots$ converges to a tiling \mathcal{T}_n with n -fold rotational symmetry. Equivalently, $\sigma^{rk}(\mathcal{P})$ converges to \mathcal{T}_n as $r \rightarrow \infty$. This tiling \mathcal{T}_n is referred to as a *fixed point* of σ^k since $\sigma^k(\mathcal{T}_n) = \mathcal{T}_n$ and the patch \mathcal{P} is called a *seed* for \mathcal{T}_n .

To illustrate the process, consider the substitution ω . The patch \mathcal{V} , shown in Figure 3a, is contained in $\omega^2(T_1)$ (see Figure 2 for verification), making \mathcal{V} a legal patch of ω . Applying ω to \mathcal{V} yields \mathcal{V}' , which is invariant under 8-fold rotation. We have $\mathcal{V}' \subset \omega(\mathcal{V}) \subset \omega^3(T_1)$, so \mathcal{V}' is also a legal patch of ω . Embedding \mathcal{V}' on the plane with its center at the origin and applying ω on \mathcal{V}' , we

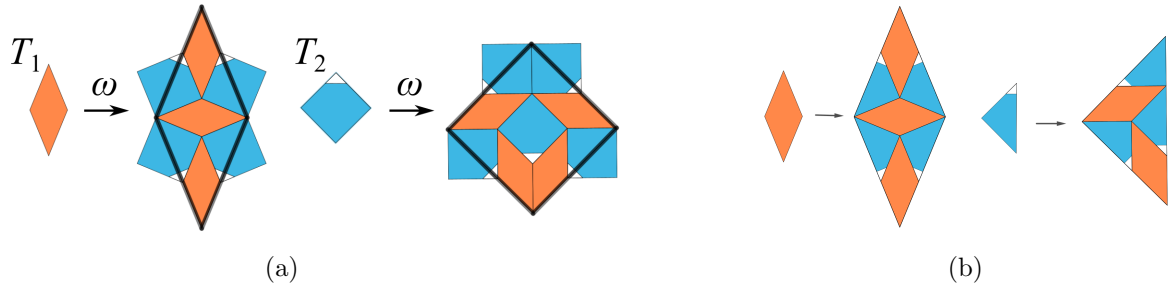


FIG. 1: Substitution rules for the Ammann-Beenker tiling.

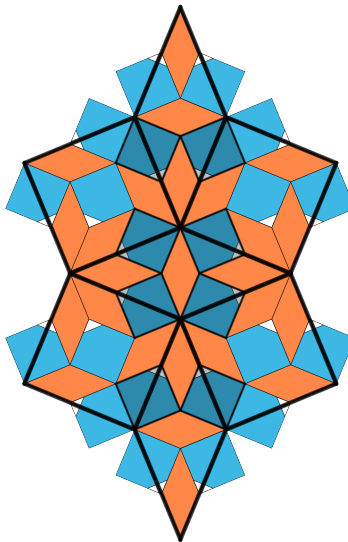


FIG. 2: The 2-order supertile of the first prototile of ω .

have $\mathcal{V}' \subset \omega(\mathcal{V}')$ as depicted in Figure 3b. Consequently, $\omega^k(\mathcal{V}')$ converges to the AB tiling, which is invariant under 8-fold rotation.

We now define an important matrix, the substitution matrix, associated with a substitution rule σ with prototiles T_1, T_2, \dots, T_m and inflation factor λ . The substitution matrix paves the way for deriving some statistical properties of tilings, which we discuss next. For the purposes of this work, we define σ as a pseudo-substitution rule where the edges of λT_i bisect any tiles not fully contained within λT_i , as in the case of ω (Figure 1a).

Let a_{ij} be the number of copies of T_i in $\sigma(T_j)$, where each copy of T_i bisected by an edge of λT_j is counted as $1/2$ so that $A(\lambda T_j) = \sum_{i=1}^m a_{ij} A(T_i)$, where $a_{ij} \in (1/2)\mathbb{Z}_{\geq 0} = \{(1/2)z \mid z \in \mathbb{Z}_{\geq 0}\}$. The *substitution matrix* of σ is defined as $M_\sigma = [a_{ij}]$. Here, $\mathbb{Z}_{\geq 0}$ denotes the set of nonnegative integers, and we denote the set of integers by \mathbb{Z} .

Clearly, M_σ is a nonnegative matrix. If, in addition, M_σ is primitive – meaning there exists a natural number k such that M_σ^k contains only positive entries – one can apply the Perron-Frobenius theorem [31] and its consequences [30, 32]. In a nutshell, the result asserts that λ^2 is a simple eigenvalue of M_σ , and it is the largest eigenvalue of M_σ in absolute value. This eigenvalue λ^2 is referred to as the PF-eigenvalue of M_σ . Furthermore, a left eigenvector \mathbf{v} corresponding to λ^2 can be scaled so that $\mathbf{v} = (A(T_1), A(T_2), \dots, A(T_m))$. Similarly, a right eigenvector \mathbf{u} can be normalized so that $\mathbf{u}^\top = (\text{freq}(T_1), \text{freq}(T_2), \dots, \text{freq}(T_m))$, where $\text{freq}(T_i)$ is the relative frequency

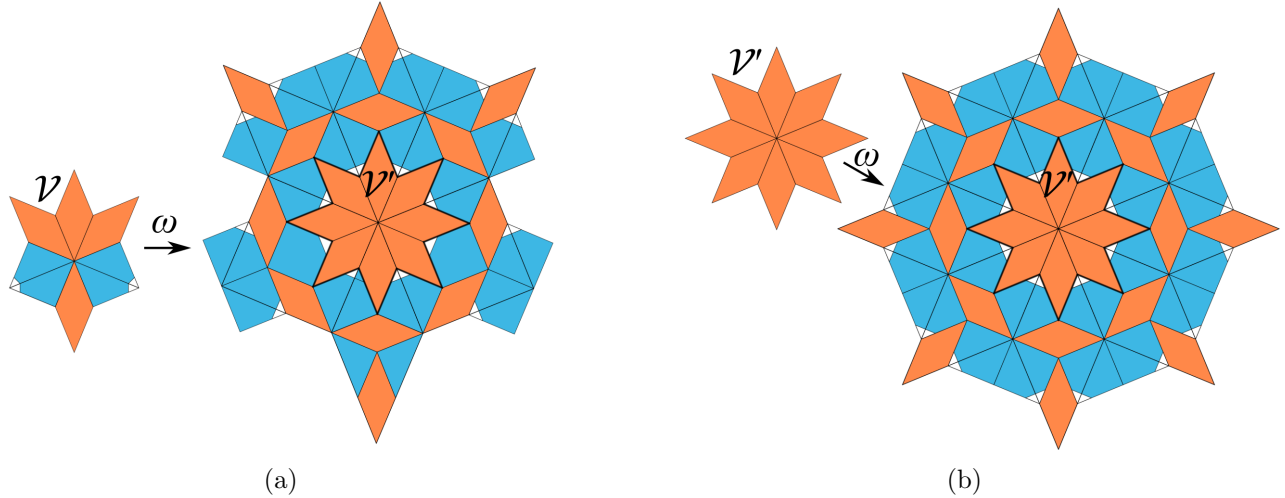


FIG. 3: The patch $\mathcal{V} \subset \omega^2(T_1)$ yields the patch \mathcal{V}' that is a seed for the AB tiling.

of T_i in any tiling corresponding to σ . Basically, $\text{freq}(T_i)$ is the ratio of the number of copies of T_i over the number of tiles in any substitution tiling corresponding to σ . Using the areas and relative frequencies of the tiles, one can obtain the area fraction $\text{af}(T_i)$ of T_i through the following formula:

$$\text{af}(T_i) = \frac{\text{freq}(T_i)A(T_i)}{\mathbf{v} \cdot \mathbf{u}}, \quad (1)$$

where $\mathbf{v} \cdot \mathbf{u}$ is the dot product of the vectors \mathbf{v} and \mathbf{u} . The area fraction $\text{af}(T_i)$ of T_i is the average number of copies of T_i per unit area in any substitution tiling corresponding to σ .

The substitution matrix of ω is given by $\begin{bmatrix} 3 & 4 \\ 2 & 3 \end{bmatrix}$ which is clearly primitive because each entry is greater than 0. The PF-eigenvalue of ω is given by $\mu^2 = 3 + 2\sqrt{2}$. The PF-left eigenvector (up to scaling) is given by $\mathbf{v} = (1, \sqrt{2})$ and its normalized right PF-right eigenvector is given by $\mathbf{u} = (2 - \sqrt{2}, \sqrt{2} - 1)^\top$. The area fraction of T_1 is

$$\text{af}(T_1) = \frac{\text{freq}(T_1)A(T_1)}{\mathbf{v} \cdot \mathbf{u}} = \frac{(2 - \sqrt{2})(1)}{(2 - \sqrt{2})(1) + (\sqrt{2} - 1)(\sqrt{2})} = \frac{1}{2}.$$

Similarly, it can be shown that $\text{af}(T_2) = \frac{1}{2}$. This means that half of the AB tiling is occupied by copies of T_1 , and half of it is occupied by T_2 .

3 Construction of the substitution rule $\sigma_{(m,n)}$

In this section, we describe the construction of our substitution rule. The inflation factor is given by $\delta_{(m,n)} = m + n\mu$, where $\mu = 1 + \sqrt{2}$, $m, n \in \mathbb{Z}_{\geq 0}$, $n \neq 0$, $(m, n) \neq (0, 1)$. The prototiles are shown in Figure 4a. Note that the polygons T_1 and T_3 are both squares with edge lengths of 1 and $\lambda = \sqrt{\frac{2+\sqrt{2}}{2}}$ units, respectively, as indicated in the figure. Meanwhile, T_2 is an isosceles triangle with legs of length λ units and base of 1 unit. It is straightforward to verify that the opening angle of T_2 is 45° . To define the edge substitution rule, we assign labels to the edges of the prototiles and to certain segment bisectors. These labels are given in Figure 4b.

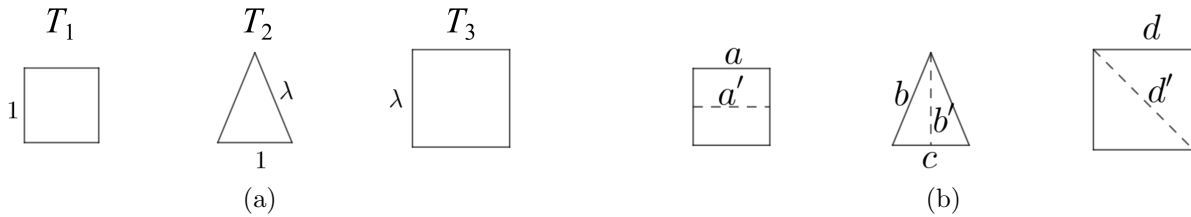


FIG. 4: (a) The prototiles; (b) edge labeling.

We note that an edge of a prototile is either of length 1 unit or λ units. Hence, if a substitution rule $\sigma_{(m,n)}$ on T_1 , T_2 and T_3 exists with inflation factor $\lambda_{(m,n)}$, $\sigma_{(m,n)}$ replaces the inflated copy of a prototile edge of length 1 by a sequence of small edges whose total length is $\delta_{(m,n)}(1) = \delta_{(m,n)} = m + n\mu$; while it replaces an inflated copy of a prototile edge of length λ by a sequence of small edges of total length $\delta_{(m,n)}(\lambda) = m\lambda + n\lambda\mu$. More precisely,

$$\delta_{(m,n)} = m + n\mu = m|a| + 2n|b'|, \quad (2)$$

where $|*|$ denotes the length of $*$. The edge a may be replaced by a' or c . Similarly,

$$\delta_{(m,n)}(\lambda) = m\lambda + n\lambda\mu = (m+n)|b| + n|d'|, \quad (3)$$

where b may be replaced by d .

Using Equations (2) and (3), the following edge substitution rules are derived for the case where $m+n$ is even. We note that the substitution rules for a and c are identical. The dissections of the inflated edges are symmetric, with edges of equal length being dissected in the same way. Specifically, if two tiles meet along the boundary of a supertile, they either intersect at a point on the boundary, meet full-edge to full-edge or overlap entirely.

$$\begin{aligned}
& (n \text{ is even}) \\
a & \mapsto \underbrace{b'-b'-b'-\dots-b'}_{n \text{ copies}} - \underbrace{a-a-a-\dots-a}_{m \text{ copies}} - \underbrace{b'-b'-b'-\dots-b'}_{n \text{ copies}} \\
& (n \text{ is odd}) \\
a & \mapsto \underbrace{b'-b'-b'-\dots-b'}_n - \underbrace{a'-a'-a'-\dots-a'}_m - \underbrace{b'-b'-b'-\dots-b'}_n \\
b & \mapsto \underbrace{b-b-b-\dots-b}_{\frac{m+n}{2}} - \underbrace{d'-d'-d'-\dots-d'}_n - \underbrace{b-b-b-\dots-b}_{\frac{m+n}{2}} \\
d & \mapsto \underbrace{d-d-d-\dots-d}_{\frac{m+n}{2}} - \underbrace{d'-d'-d'-\dots-d'}_n - \underbrace{d-d-d-\dots-d}_{\frac{m+n}{2}}
\end{aligned}$$

FIG. 5: Edge substitution rule for the case $m + n$ is even; the substitution for c is the same as a .

After dissecting the edges of $\delta_{(m,n)}T_i$ according to the rules described in Figure 5, the approach is to dissect $\delta_{(m,n)}T_i$ into regions that can each be clearly dissected into copies of a single prototile. These regions are determined by applying basic geometry, taking into consideration both the interior angles and lengths, as well as the area decomposition of $A(\delta_{(m,n)}T_i)$.

Figures 6-9 show the decompositions into regions corresponding to the cases $m = n$, $m > n$, $m = 0$, and $m < n$, respectively, when $m + n$ is even (where we discuss an example of an odd case in section 5). Each gray region can be dissected further into congruent copies of T_1 , each blue region into copies of T_2 , and each orange region into copies of T_3 . The number of copies of a prototile within each region are highlighted within selected regions or adjacent to the prototile, with edge lengths of regions also marked. These dissections naturally define a pseudo-substitution rule, which we denote by $\sigma_{(m,n)}$.

The properties of $\sigma_{(m,n)}$ are evident in the dissections. Specifically, $\sigma_{(m,n)}$ preserves the symmetry group of the prototile, making it unnecessary to decorate the tiles. Furthermore, the substitution rule $\sigma_{(m,n)}$ generates a tiling $\mathcal{T}_{(m,n)}$ with 8-fold rotational symmetry. For each case, the seed of $\mathcal{T}_{(m,n)}$ is a central patch of $\sigma_{(m,n)}(T_3)$ consisting of eight copies of T_2 and exhibiting D_8 symmetry, the dihedral group of order 16.

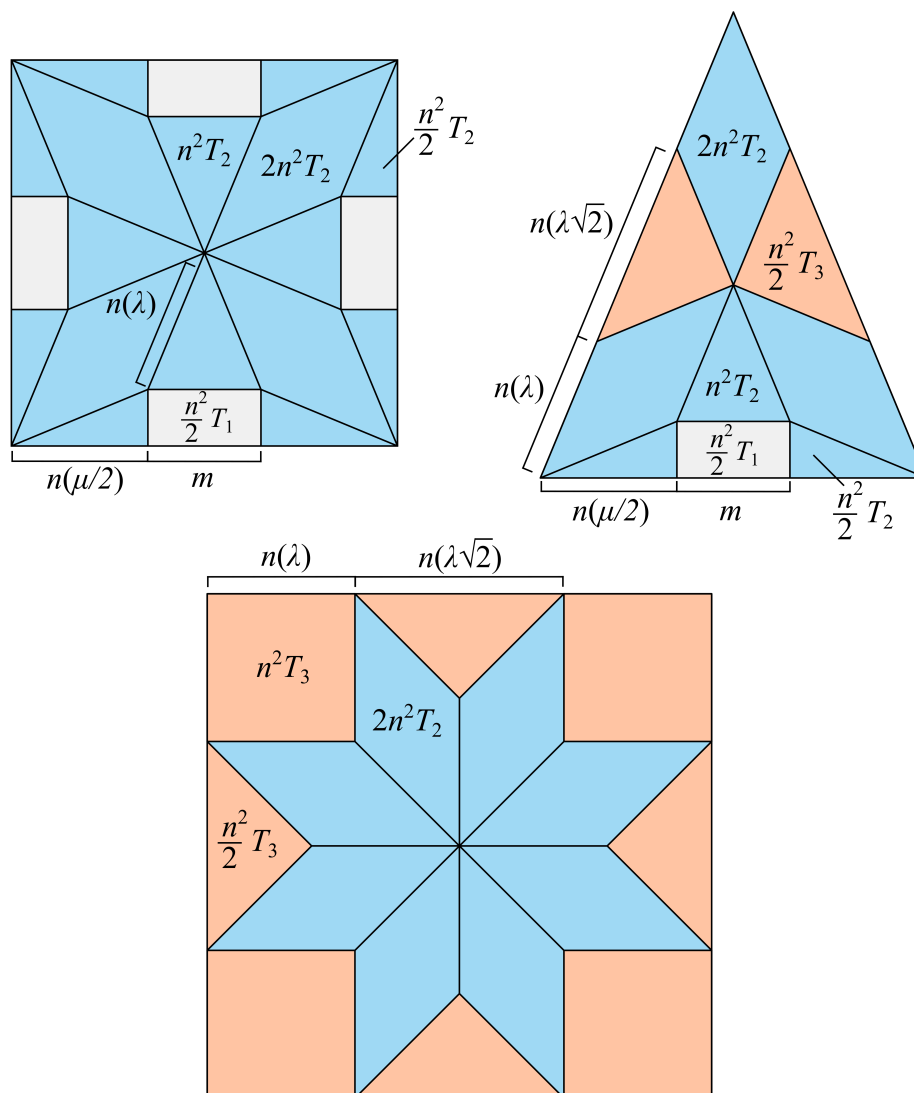


FIG. 6: The dissection of $\delta_{(n,n)}T_i$ into regions, $i \in \{1, 2, 3\}$. Each region can be dissected into copies of a single prototile, with the number of tiles indicated within selected regions.

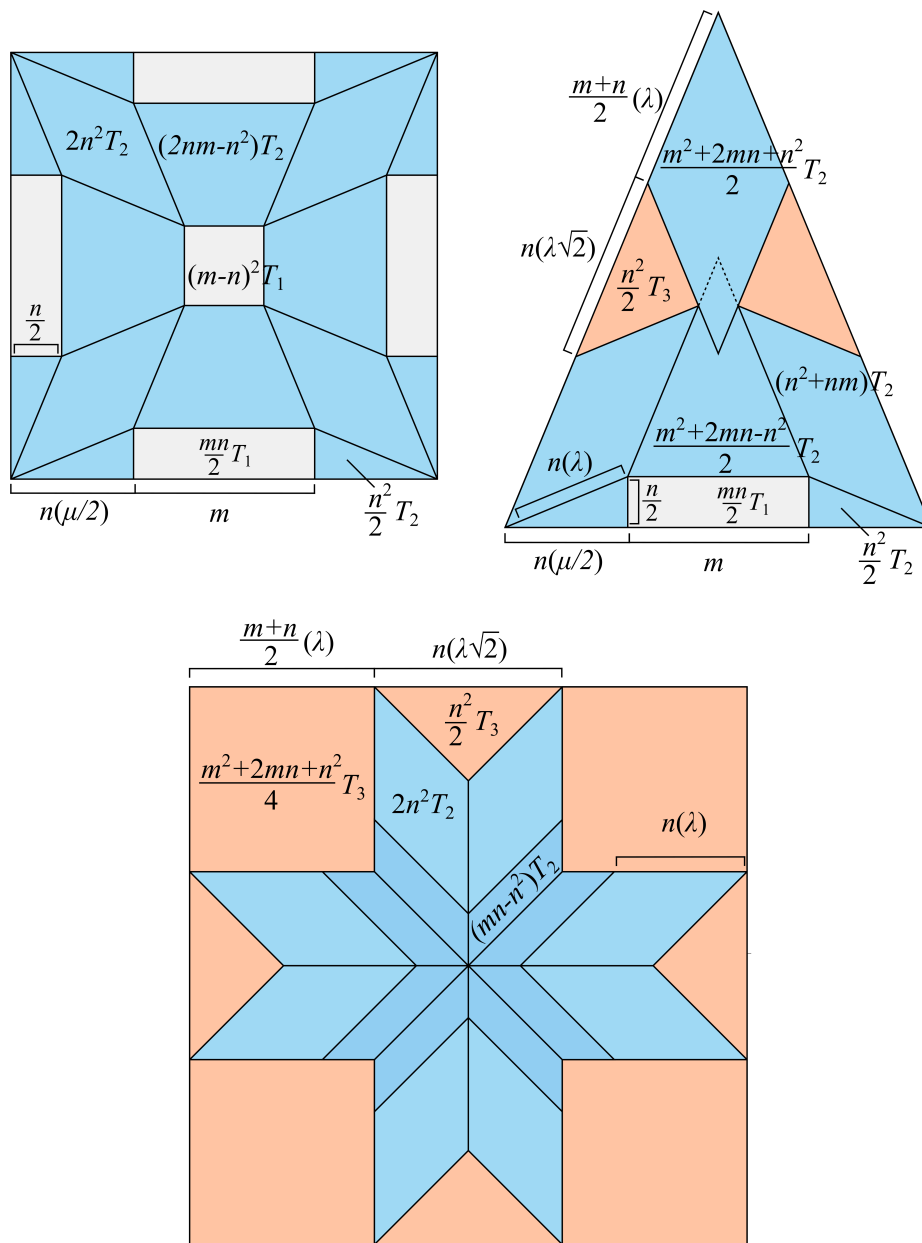


FIG. 7: The dissection of $\delta_{(m,n)} T_i$, $i \in \{1, 2, 3\}$, $m > n$.

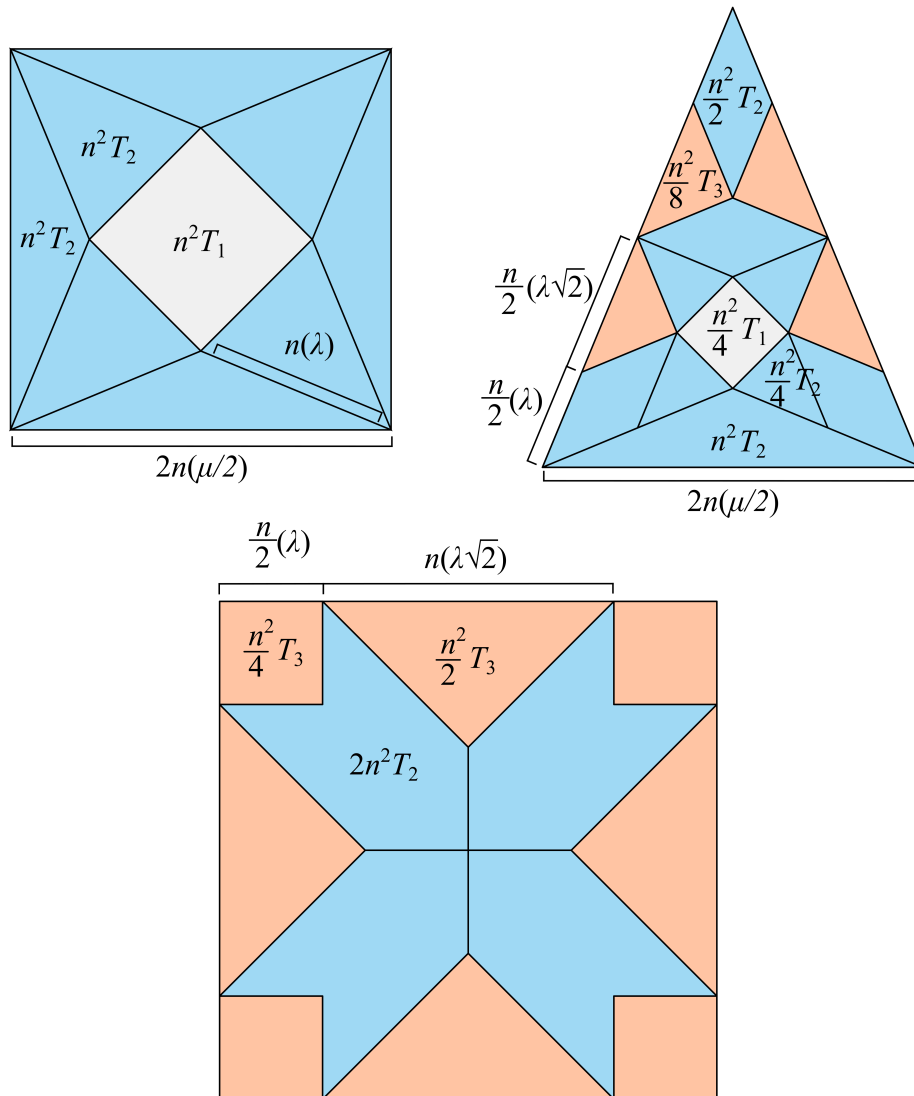


FIG. 8: The dissection of $\delta_{(m,n)} T_i$, $i \in \{1, 2, 3\}$, $m = 0$.

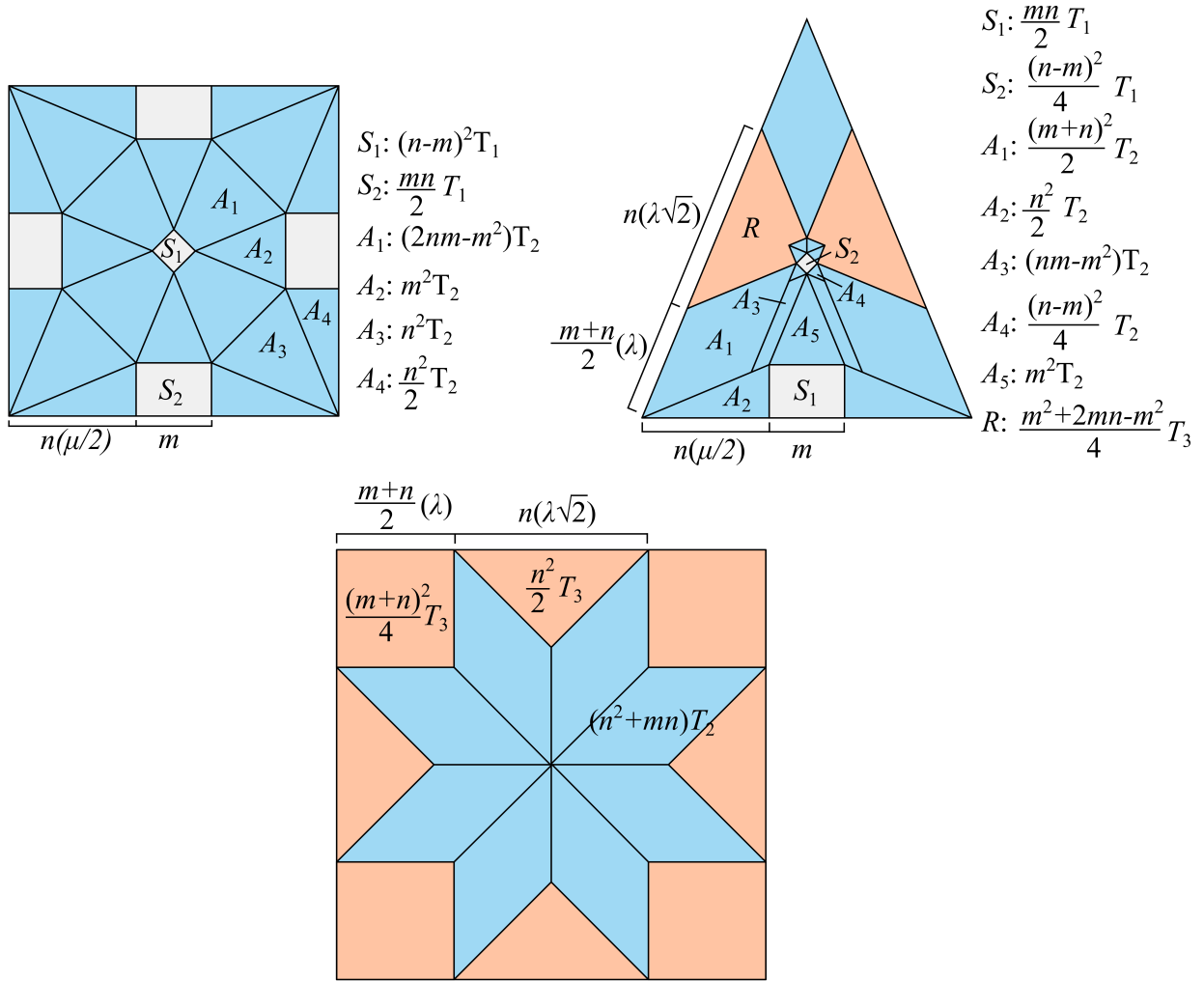


FIG. 9: The dissection of $\delta_{(m,n)} T_i$, $i \in \{1, 2, 3\}$, $0 < m < n$.

4 Statistical properties

4.1 Area fractions

By counting the occurrences of each prototile within $\delta_{(m,n)}T_i$, as given in the previous section, we obtain the substitution matrix associated to $\sigma_{(m,n)}$ as follows.

$$M_{(m,n)} = \begin{bmatrix} m^2 + n^2 & \frac{mn}{2} & 0 \\ 8mn + 8n^2 & m^2 + 4mn + 3n^2 & 8mn + 8n^2 \\ 0 & n^2 & m^2 + 2mn + 3n^2 \end{bmatrix} + \begin{bmatrix} 0 & b & 0 \\ 0 & 4b & 0 \\ 0 & -2b & 0 \end{bmatrix}, \quad (4)$$

where $b = 0$ for $m \geq n$ and $b = \frac{(n-m)^2}{4}$ for $0 \leq m < n$.

It is straightforward to verify that all entries of $M_{(m,n)}^2$ are positive, confirming that $M_{(m,n)}$ is primitive. As discussed in Section 2, the left eigenvector and the normalized right eigenvector of $M_{(m,n)}$ represent the areas (up to scaling) and the relative frequencies of the prototiles, respectively. These values yield the area fractions of the prototiles (see Equation (1)), which are summarized in Table I.

Case	Prototile	Area	Relative Frequency	Area Fraction
$m \geq n$	T_1	1	$\frac{m(2 - \sqrt{2})}{2(m+n) + (3m+4n)}$	$\frac{m(2 - \sqrt{2})}{4m + 4n + 2\sqrt{2}n}$
	T_2	$\frac{1 + \sqrt{2}}{4}$	$\frac{4\sqrt{2}(m+n)}{2(m+n) + (3m+4n)}$	$\frac{(m+n)(2 + \sqrt{2})}{4m + 4n + 2\sqrt{2}n}$
	T_3	$\frac{2 + \sqrt{2}}{2}$	$\frac{2n}{2(m+n) + (3m+4n)}$	$\frac{n(2 + \sqrt{2})}{4m + 4n + 2\sqrt{2}n}$
$0 \leq m < n$	T_1	1	$\frac{(m^2 + n^2)(2 - \sqrt{2})}{4(n^2 + mn) + (7n^2 + 8mn - m^2)}$	$\frac{(m^2 + n^2)(2 - \sqrt{2})}{8n^2 + 8mn - 2m^2\sqrt{2} + 4\sqrt{2}mn + 2\sqrt{2}n}$
	T_2	$\frac{1 + \sqrt{2}}{4}$	$\frac{8(n^2 + mn)\sqrt{2}}{4(n^2 + mn) + (7n^2 + 8mn - m^2)}$	$\frac{2(n^2 + mn)(2 + \sqrt{2})}{8n^2 + 8mn - 2m^2\sqrt{2} + 4\sqrt{2}mn + 2\sqrt{2}n}$
	T_3	$\frac{2 + \sqrt{2}}{2}$	$\frac{2(n^2 + 2mn - m^2)}{4(n^2 + mn) + (7n^2 + 8mn - m^2)}$	$\frac{(n^2 + 2mn - m^2)(2 + \sqrt{2})}{8n^2 + 8mn - 2m^2\sqrt{2} + 4\sqrt{2}mn + 2\sqrt{2}n}$

TABLE I: The relative frequencies and area fractions of the prototiles of $\sigma_{(m,n)}$.

For each case in Table I, we see that $\text{af}(T_2) > \text{af}(T_3) > \text{af}(T_1)$. More precisely,

$$(3 + 2\sqrt{2})\text{af}(T_1) - \text{af}(T_2) + \text{af}(T_3) = 0. \quad (5)$$

As discussed in [19], Equation (5) specifies the condition under which a tiling of the three prototiles exhibits zero strain in perpendicular space, as expected from our construction. While the authors of [19] derived this condition by considering the hyperslope of each tile in a globally uniform tiling, we show that it can also be obtained directly via the substitution matrix (4).

4.2 An example of vertex types and projection windows

We can consider the structure of a given tiling via its vertex stars. The *vertex star* of a vertex in a tiling corresponds to the patch of all tiles meeting at the vertex. We do so here in order to demonstrate the changes in the number of vertex stars (up to rotations and reflections) that occur when altering (m, n) . A generalised approach to this issue across our entire family of tilings constitutes further, extensive work, as we have multiple tilings and many possible variations (see next section). However, to provide an example for the basis of such work, we choose the simplest of cases i.e., where $\sigma_{(n,n)}$ for $n = 1, 2$.

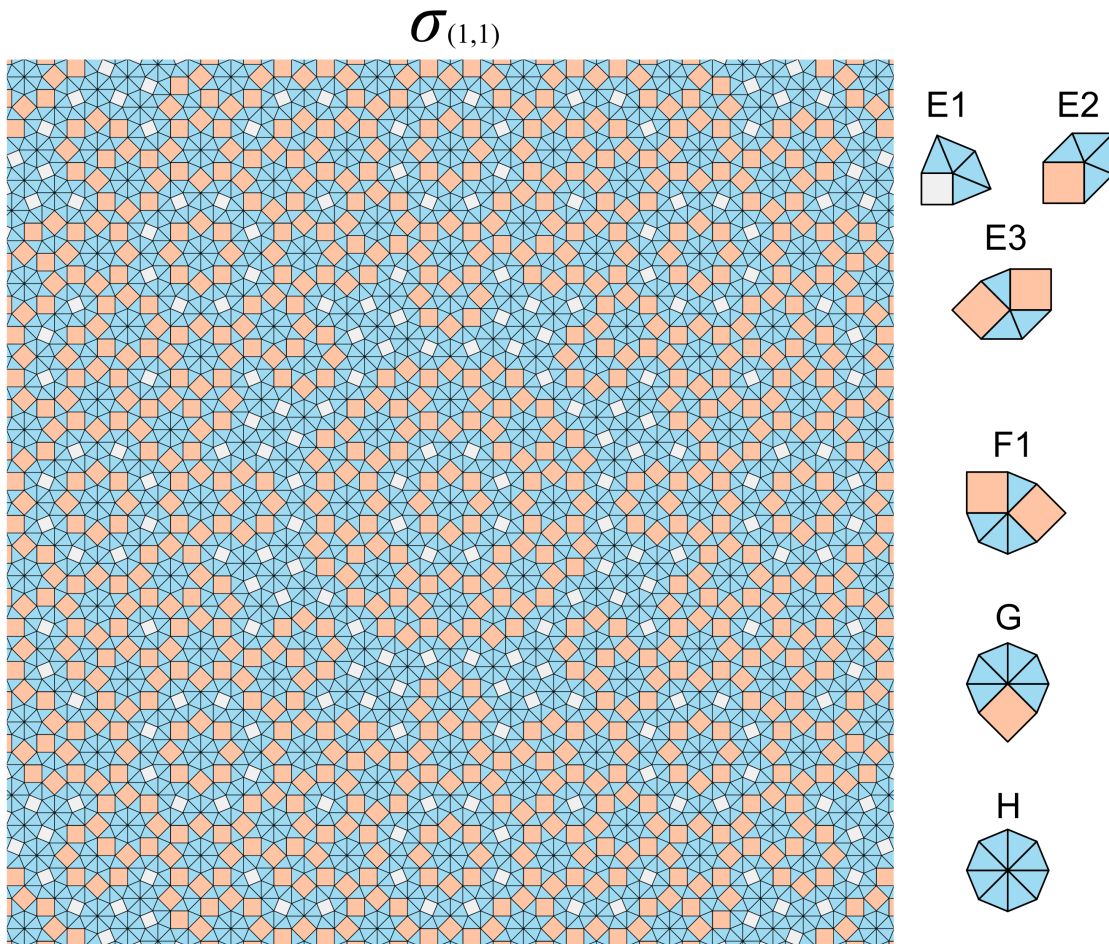


FIG. 10: Left: A legal patch of $\sigma_{(1,1)}$ initiated by substituting T_3 . Right: the six vertex stars found across $\sigma_{(1,1)}$.

Figure 10 shows a legal patch of $\sigma_{(1,1)}$ obtained by iterating the substitution on T_3 . The six vertex stars that are found across any tiling associated to $\sigma_{(1,1)}$ are shown on the right hand side, labelled with letters corresponding to their coordination number (E = 5, F = 6, etc.), with some vertex stars also numbered to differentiate between equal coordination numbers. As discussed in [33], a vertex star of a substitution tiling with convex prototiles can occur in one of the three locations: within the interior of a 1-order supertile, along the boundary between two 1-order supertiles, or as a central patch in the image of a vertex star under the substitution rule. If every vertex star appears exclusively in the interior of a 1-order supertile and nowhere else in

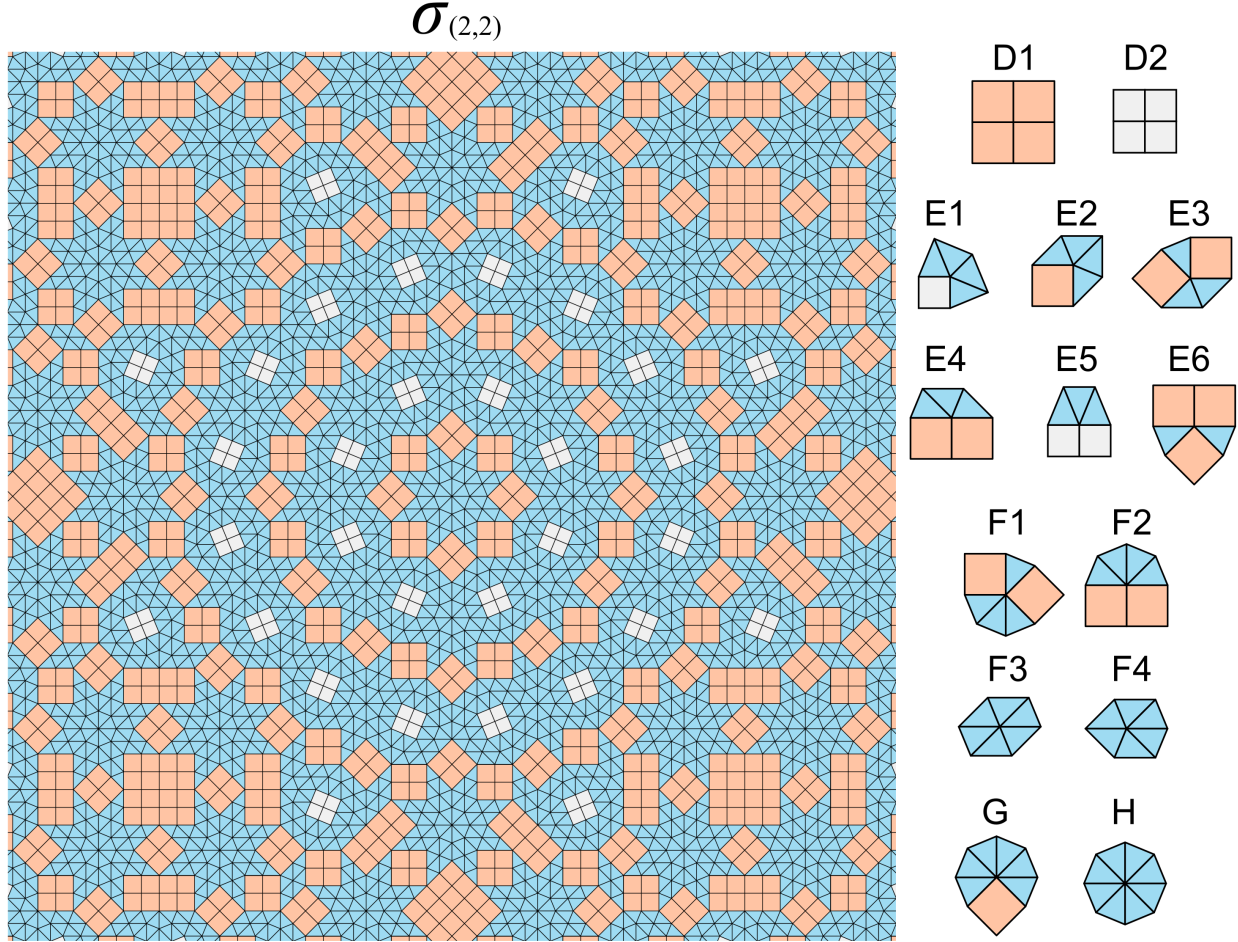


FIG. 11: Left: A legal patch of $\sigma_{(2,2)}$ initiated by substituting T_3 . Right: the fourteen vertex stars found across $\sigma_{(2,2)}$.

the tiling, its area fraction - the average number of copies of that vertex star per unit area in any tiling associated to substitution rule - can be derived from the area fractions of the prototiles. For example, the vertex star E1 appears eight times in every copy of $\sigma_{(1,1)}(T_1)$ and twice in every copy of $\sigma_{(1,1)}(T_2)$, with no occurrences elsewhere in the tiling. Given the area fractions of T_1 and T_2 for the case $m = n = 1$ (see Table I), we obtain:

$$\text{af}(\text{E1}) = \frac{8\text{af}(T_1) + 2\text{af}(T_2)}{\delta_{(1,1)}^2} = \frac{59 - 41\sqrt{2}}{7} \approx 0.1453. \quad (6)$$

Figure 11 then shows a legal patch of $\sigma_{(2,2)}$. The number of vertex stars increases to fourteen, where they are labelled in the same manner as Figure 10. This outcome is expected as the 1-order supertiles are larger. Moreover, due to the way the substitution rule is defined, the vertex stars in $\sigma_{(1,1)}$ also appear in $\sigma_{(2,2)}$. Thus, given that the number of prototiles is finite, one can anticipate that, for some $k \geq 3$, $\sigma_{(k-1,k-1)}$ and $\sigma_{(k,k)}$ will contain the same number of vertex stars.

We can also analyse the vertex arrangements across the tilings using a higher-dimensional view. Here, each tiling is represented by a subset of points belonging to a periodic lattice in a higher-dimensional superspace. This superspace is split into two: a physical or ‘parallel’ space, which the tiling vertex arrangements occupy, and a complementary perpendicular space. Projected lattice

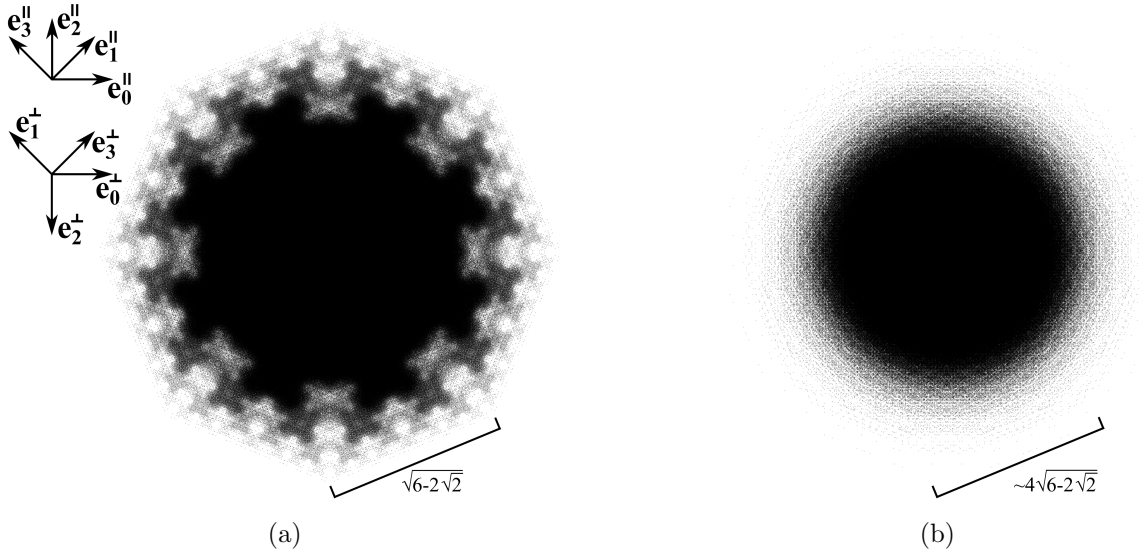


FIG. 12: (a) The perpendicular space window of $\sigma_{(1,1)}$. Inset are the parallel and perpendicular space vectors used to index the $\sigma_{(1,1)}$ vertices; (b) the $\sigma_{(2,2)}$ window, which is approximately four times as large as the $\sigma_{(1,1)}$ window.

points which fall onto perpendicular space ‘windows’ correspond directly to the physical space vertices.

Following the ‘lifting’ procedure employed in [19], the windows of $\delta_{(1,1)}$, $\delta_{(2,2)}$ are constructed by indexing each vertex with respect to four physical space vectors ($\mathbf{e}_0^{\parallel}, \dots, \mathbf{e}_3^{\parallel}$), shown in the inset of Figure 12a, such that each vertex can be represented as a 4-tuple of integers n , or, as a point on a 4D lattice. Then, the perpendicular space points which fall on the windows are constructed by $n \cdot \mathbf{e}^{\perp}$, where $\mathbf{e}^{\perp} = (\mathbf{e}_0^{\perp}, \dots, \mathbf{e}_3^{\perp})$ are the associated perpendicular space vectors, also shown in the inset of 12a.

Figure 12 shows the perpendicular space windows for $\sigma_{(1,1)}$ and $\sigma_{(2,2)}$, which are plotted considering 4×10^6 and 7×10^6 vertices respectively. Appendix A also shows a decomposition of the $\sigma_{(1,1)}$ window into the sub-regions which define the specific vertex types shown in Figure 10. The points densely fill areas which appear to be bounded by octagons: the edge length of the octagonal boundary of $\sigma_{(1,1)}$ is $\sqrt{6 - 2\sqrt{2}}$ (or $\lambda/(\cos \pi/8)$), while the $\sigma_{(2,2)}$ window is approximately 4 times as large. Given this limited example, we can naively assume that as the division of $\sigma_{(n,n)}$ scales with n^2 , the edge length of the octagonal boundary also scales as $n^2 \sqrt{6 - 2\sqrt{2}}$. This suggests that for the $\sigma_{(n,n)}$ family the perpendicular space window simply expands as n increases in order to admit an increased density of projected 4D points – as opposed to representing a different plane in higher-dimensional space. Proof of this hypothesis, and whether this condition (or some variation) holds for the $\sigma_{(m,n)}$ tilings will be explored in further work.

5 Variants of $\sigma_{(m,n)}$ and the case $m+n$ is odd

The number b in Equation (4) illustrates the area relation $2A(T_3) = A(T_1) + 4A(T_2)$. This relationship is useful in finding a variant of the constructed substitution by replacing two copies of T_3 in a 1-order supertile with one copy of T_1 and four copies of T_2 , or vice versa. As a result, $M_{(m,n)}$ can be further generalized to include the variants of $\sigma_{(m,n)}$, as shown below:

$$M'_{(m,n)} = \begin{bmatrix} m^2 + n^2 & \frac{mn}{2} & 0 \\ 8mn + 8n^2 & m^2 + 4mn + 3n^2 & 8mn + 8n^2 \\ 0 & n^2 & m^2 + 2mn + 3n^2 \end{bmatrix} + \begin{bmatrix} a & b & c \\ 4a & 4b & 4c \\ -2a & -2b & -2c \end{bmatrix}, \quad (7)$$

where $a, b, c \in \frac{1}{2}\mathbb{Z}$.

A variant can also be found by simply rearranging the tiles to arrive at a different definition of the 1-order supertiles.

As an illustration, let us consider the case $m = n = 2$. Figure 13 displays two variants of each $\sigma_{(2,2)}(T_i)$, with the corresponding a, b , and c explicitly indicated. Since boundaries of equal length match, we can form $2 \times 2 \times 2 = 8$ distinct variants of $\sigma_{(2,2)}$ from the given 1-order supertiles.

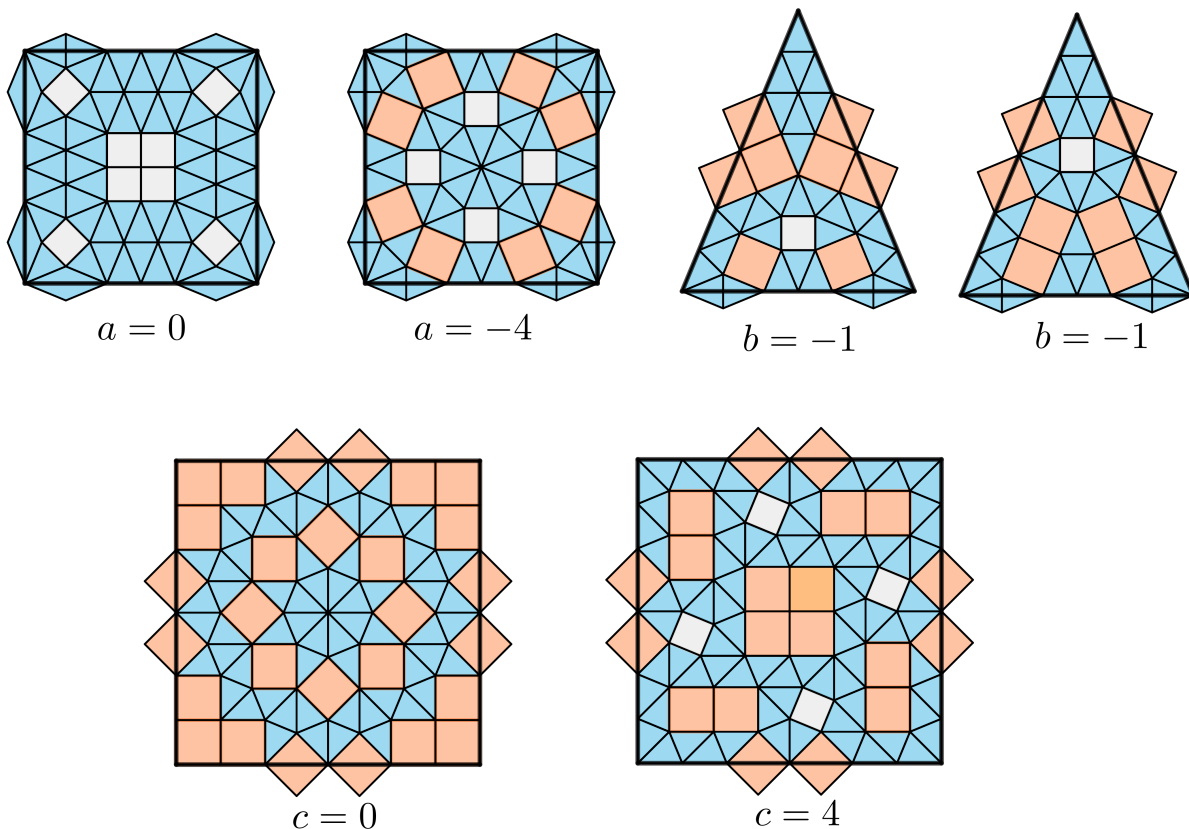


FIG. 13: Some variants of $\sigma_{(2,2)}(T_i)$, $i \in \{1, 2, 3\}$.

For simplicity, we did not address the case where $m+n$ is odd in Section 3. However, we believe that analogous subcases to those in the even case of $m+n$ will arise here as well. For instance the case $m < n$, where m is even, is shown in Figure 14. Unlike when $m+n$ is even, the edge substitution rules for edges b and d are likely to be non-symmetric. As described in

Equation (3), $\delta_{(m,n)}|b|$ will consist of $m + n$ copies of b or d and n copies of d' . Since $m + n$ is odd, these $m + n$ copies cannot be evenly divided to produce a symmetric edge substitution rule, in contrast to the even case.

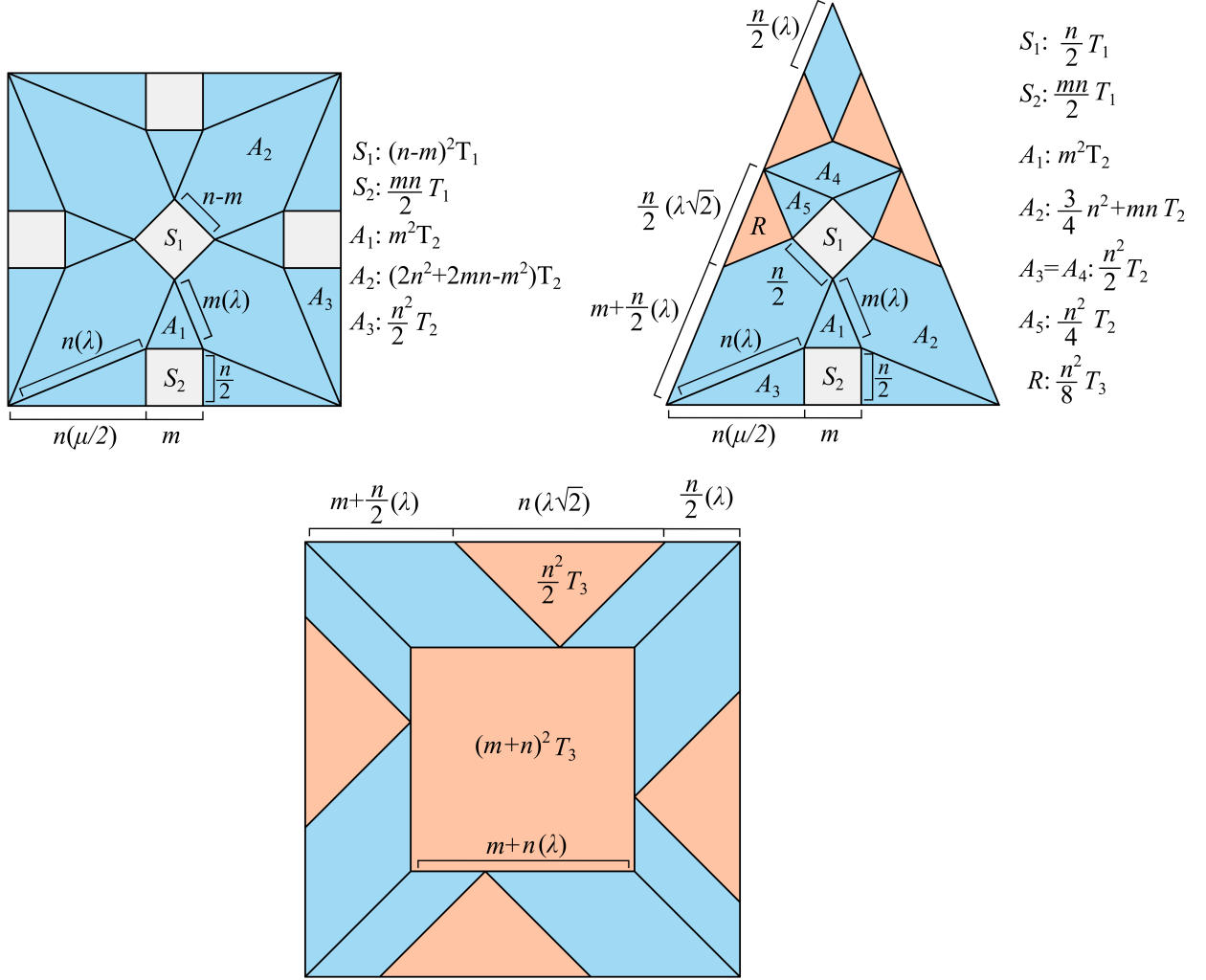


FIG. 14: Dissection of $\delta_{(m,n)}T_i$, $i \in \{1, 2, 3\}$, $m + n = \text{odd}$, $m = \text{even}$.

6 Comparison with Existing Tilings

6.1 QC8 Tilings

In addition to Equation (5), formulas for the area fractions of the prototiles were also derived for the tilings in [19]. These area fractions, denoted as σ , τ , and Σ , correspond to the prototiles T_1 , T_2 , and T_3 , respectively, and are expressed in Equations (8)–(10). These formulae depend on the fraction of small particles, x_S . It is of particular interest to compare these area fractions with those obtained in this study. By solving the system of equations $\sigma = \text{af}(T_1)$, $\tau = \text{af}(T_2)$, and $\Sigma = \text{af}(T_3)$, we derived a formula for x_S that yields identical area fractions to those found in this work, such that our tilings directly represent non-random analogues to those found in [19]. For the case where $m \geq n$, the formula is provided in Equation (11), and for the case where $0 \leq m < n$, it is presented in Equation (12).

$$\sigma = \frac{-(4 + \sqrt{2})x_S + 4}{6 - 4x_S} \quad (8)$$

$$\tau = \frac{-(8 + 5\sqrt{2})x_S + 4\sqrt{2} + 7}{6 - 4x_S} \quad (9)$$

$$\Sigma = \frac{2(4 + 3\sqrt{2})x_S - 4\sqrt{2} - 5}{6 - 4x_S} \quad (10)$$

$$x_S = \frac{m(2 + 3\sqrt{2}) + 4n(2 + \sqrt{2})}{4m(1 + \sqrt{2}) + 2(5 + 3\sqrt{2})} \quad (11)$$

$$x_S = \frac{n^2(10 + 7\sqrt{2}) - m^2(6 + \sqrt{2}) + 8mn(2 + \sqrt{2})}{2n^2(7 + 5\sqrt{2}) - 2m^2(3 + \sqrt{2}) + 4mn(5 + 3\sqrt{2})} \quad (12)$$

6.2 The AB tiling and Watanabe-Ito-Soma tiling

Given a tiling corresponding to $\sigma_{(m,n)}$, it is possible to derive a new tiling by applying a local replacement rule. More precisely, all copies of T_1 can be removed from the original tiling to produce a new tiling composed exclusively of tiles congruent to T_2 and T_3 . If the rule preserves the full-edge to full-edge property, the new tiling can be viewed as a tiling of rhombi (formed by two copies of T_2) and squares, which is closely related to the AB tiling [1, 29] and the Watanabe-Ito-Soma tiling [2].

Consider, for instance, the substitution $\sigma_{(1,1)}$. One of its legal patches, \mathcal{A} (see Figure 15), consists of one copy of T_1 and seven copies of T_2 . As shown in Figure 15, $\text{supp}(\mathcal{A})$ can be dissected into three copies of T_2 and two copies of T_3 , forming a new patch denoted as \mathcal{A}' . Any tiling \mathcal{T} arising from $\sigma_{(1,1)}$ is a union of copies of n -order supertiles of the prototiles. In particular, it is a union of copies of the 2-order supertiles shown Figure 16. When these copies are joined together to form \mathcal{T} , it is clear that \mathcal{T} can be partitioned into copies of T_2 , T_3 and \mathcal{A} . By systematically replacing every copy of \mathcal{A} in \mathcal{T} with \mathcal{A}' , a new tiling \mathcal{T}' of rhombi and squares is constructed. A patch of \mathcal{T}' is displayed in Figure 17.

It is important to emphasize that the new tiling \mathcal{T}' is distinct from both the Ammann-Beenker (AB) tiling and the Watanabe-Ito-Soma tiling. Figure 18 shows two vertex stars that appear in \mathcal{T}' but do not appear in the AB tiling. One can verify this in Example 7.9 of [30], where the six vertex stars of the AB tiling are listed. It is also not difficult to verify that the first vertex configuration does not appear in the Watanabe-Ito-Soma tiling. See, for instance, [34], which shows a large patch of the tiling.

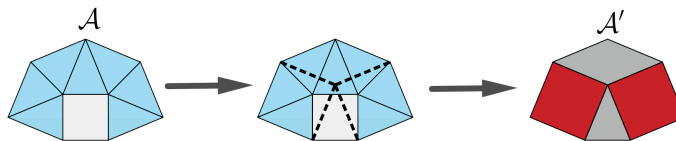


FIG. 15: Replacement rule.

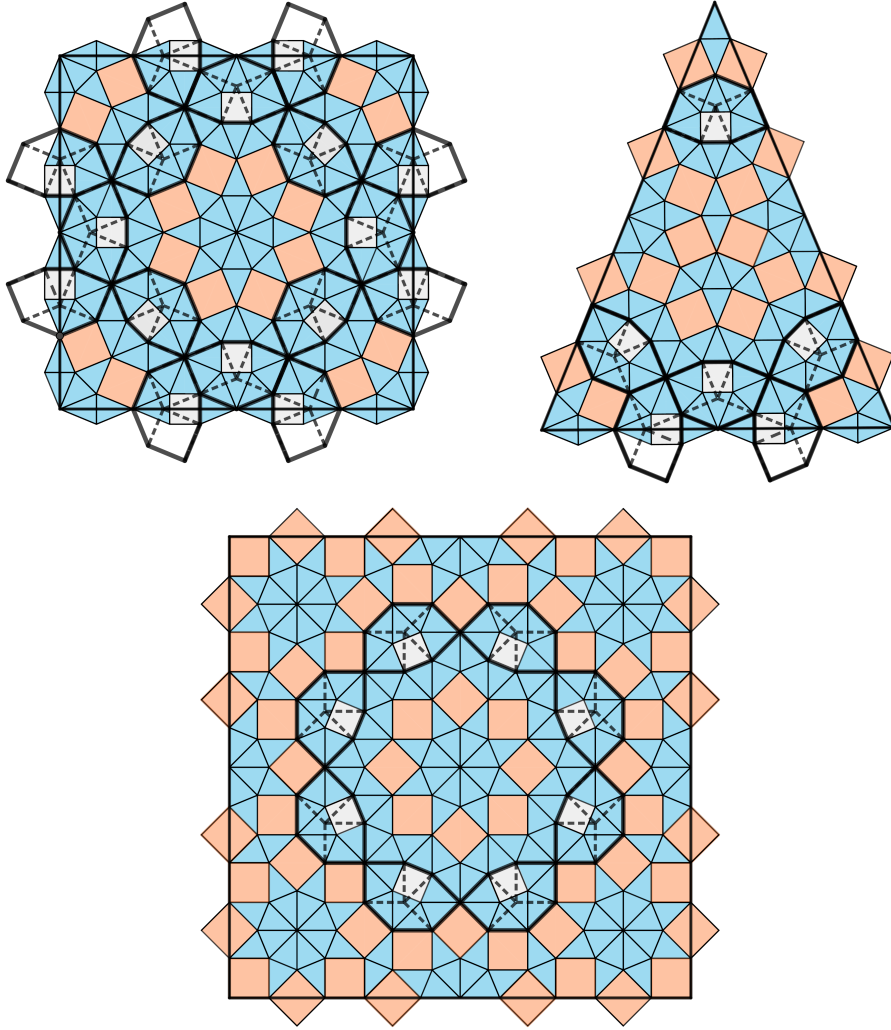


FIG. 16: The 2-order supertiles of $\sigma_{(1,1)}$, in which copies of \mathcal{A} are enclosed by thick edges.

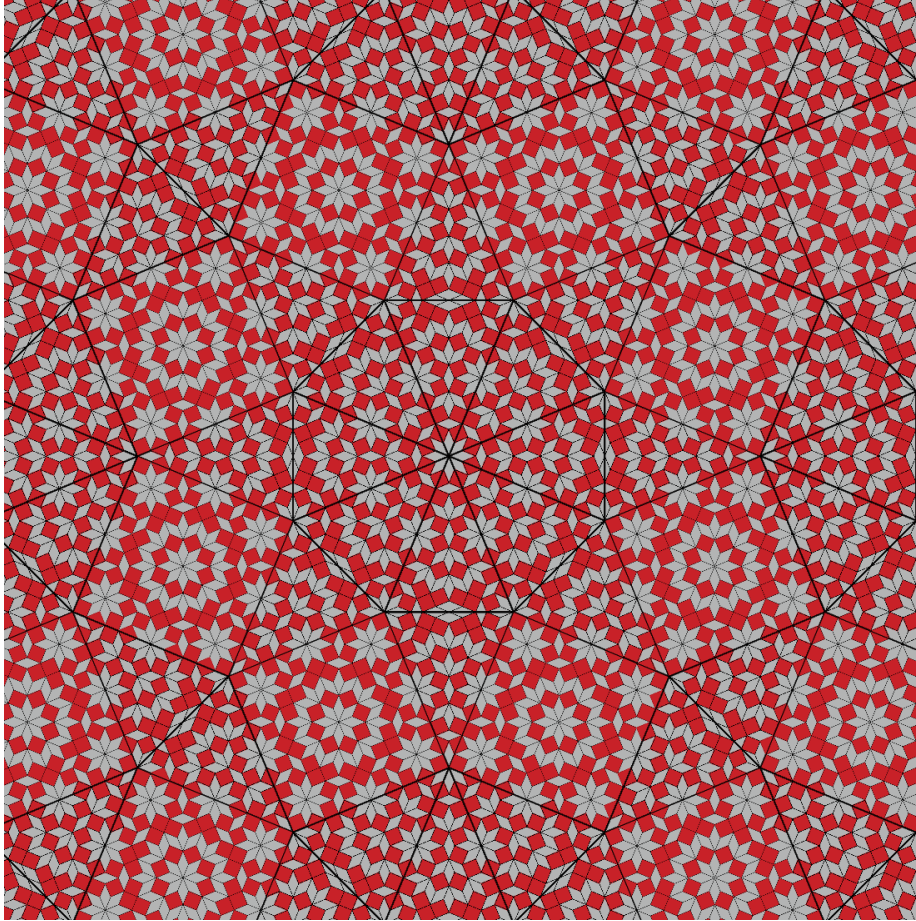


FIG. 17: A patch of the tiling \mathcal{T}' derived from \mathcal{T} via the replacement rule described in Figure 15.

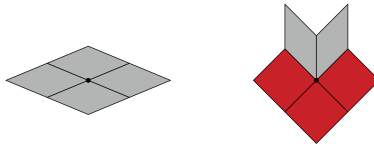


FIG. 18: Some vertex stars of \mathcal{T}'

7 Conclusions and outlook

We have presented a new family of tilings with octagonal symmetry, consisting of three prototiles. We have demonstrated how to decompose these prototiles according to two non-negative integers, m and n , with four distinct cases characterised by the relative values of these integers. In addition, we presented the statistical properties of our tilings, demonstrated the structural variants one can obtain, and compared our tiling structures to existing octagonal tilings. Future work will focus on defining cases where $m+n$ is odd, and further exploring the projection windows obtained in perpendicular space across the entire tiling family.

The introduction of our family of tilings and the generalized method with which to produce them points to two immediate applications. First, they provide additional tools for the character-

ization of the binary hard-sphere phases of matter as described in [19], and similar phases. Here, random-tiling quasicrystals are decorated with the three prototiles we have used, producing specific tile distributions which are dependent on sphere size and ratio. Should a tiling exist in our family which matches a given tile distribution observed in these systems, we can consider whether our ordered tiling describes a singular, low-entropy, energetically dominated ground state, or is simply one of many degenerate entropically dominated states. Second, the wide array of physical models that have been explored on tilings can similarly be applied to our family. Of particular interest would be the comparison to the magnetic, electronic, and statistical properties of a given tiling and the archetypal Ammann-Beenker [7–15], amongst others.

Acknowledgments

The authors express their gratitude to Marianne Impérator-Clerc, Frank Smalenburg and Andrea Plati for helpful discussions. SC acknowledges that this work was supported by EPSRC grant EP/X011984/1.

A $\sigma_{(1,1)}$ window sub-regions

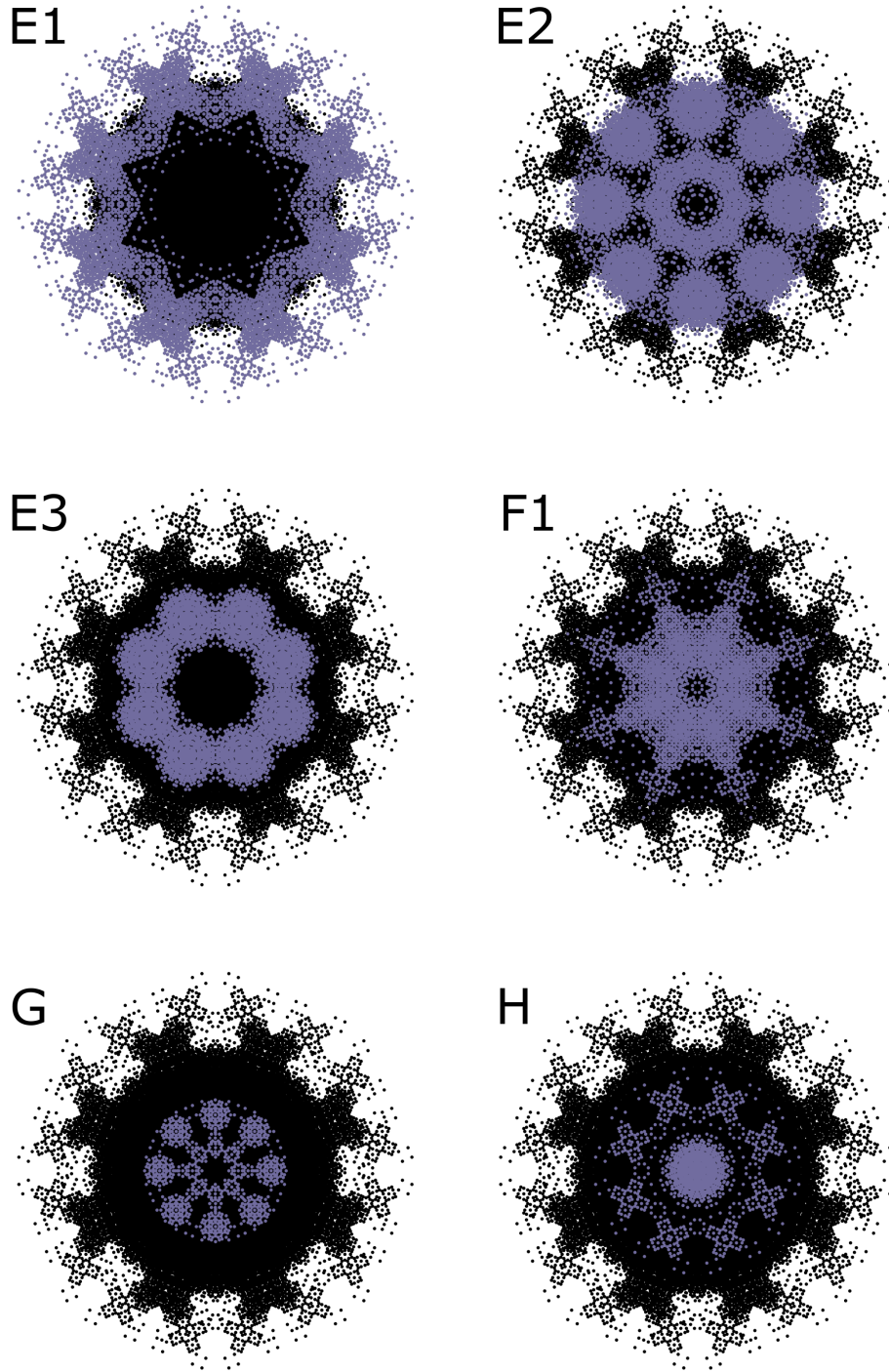


FIG. A1: Sub-regions of the perpendicular space window of $\sigma_{(1,1)}$. The window points are plotted in black, with the specific vertex sub-regions overlaid in purple. Each sub-region is labelled with respect to the vertex nomenclature in Figure 10.

-
- [1] R. Ammann, B. Grünbaum, and G. C. Shephard, Aperiodic tiles, *Discrete & Computational Geometry* **8**, 1 (1992).
 - [2] Y. Watanabe, M. Ito, and T. Soma, Nonperiodic tessellation with eightfold rotational symmetry, *Acta Crystallographica Section A: Foundations of Crystallography* **43**, 133 (1987).
 - [3] J. E. Socolar, Simple octagonal and dodecagonal quasicrystals, *Physical Review B* **39**, 10519 (1989).
 - [4] J. Block and S. Weinberger, Aperiodic tilings, positive scalar curvature, and amenability of spaces, *Journal of the American Mathematical Society* **5**, 907 (1992).
 - [5] C. Oguey, M. Duneau, and A. Katz, A geometrical approach of quasiperiodic tilings, *Communications in mathematical physics* **118**, 99 (1988).
 - [6] C. Sire, R. Mosseri, and J.-F. Sadoc, Geometric study of a 2d tiling related to the octagonal quasiperiodic tiling, *Journal de Physique* **50**, 3463 (1989).
 - [7] S. Thiem and J. Chalker, Magnetism in rare-earth quasicrystals: Rkky interactions and ordering, *Europhysics Letters* **110**, 17002 (2015).
 - [8] S. Thiem and J. Chalker, Long-range magnetic order in models for rare-earth quasicrystals, *Physical Review B* **92**, 224409 (2015).
 - [9] R. N. Araújo, C. C. Bellinati, and E. C. Andrade, Fragile magnetic order in metallic quasicrystals, *Physical Review B* **110**, 165131 (2024).
 - [10] N. Mace, A. Jagannathan, and M. Duneau, Quantum simulation of a 2d quasicrystal with cold atoms, *Crystals* **6**, 124 (2016).
 - [11] T. Fukushima, N. Takemori, S. Sakai, M. Ichioka, and A. Jagannathan, Supercurrent distribution in real-space and anomalous paramagnetic response in a superconducting quasicrystal, *Physical Review Research* **5**, 043164 (2023).
 - [12] A. Koga, Superlattice structure in the antiferromagnetically ordered state in the hubbard model on the ammann-beenker tiling, *Physical Review B* **102**, 115125 (2020).
 - [13] N. Macé, A. Jagannathan, P. Kalugin, R. Mosseri, and F. Piéchon, Critical eigenstates and their properties in one-and two-dimensional quasicrystals, *Physical Review B* **96**, 045138 (2017).
 - [14] S. Singh, J. Lloyd, and F. Flicker, Hamiltonian cycles on ammann-beenker tilings, *Physical Review X* **14**, 031005 (2024).
 - [15] J. Lloyd, S. Biswas, S. H. Simon, S. Parameswaran, and F. Flicker, Statistical mechanics of dimers on quasiperiodic ammann-beenker tilings, *Physical Review B* **106**, 094202 (2022).
 - [16] J. A. Millan, D. Ortiz, and S. C. Glotzer, Effect of shape on the self-assembly of faceted patchy nanoplates with irregular shape into tiling patterns, *Soft Matter* **11**, 1386 (2015).
 - [17] C. R. Iacovella, A. S. Keys, and S. C. Glotzer, Self-assembly of soft-matter quasicrystals and their approximants, *Proceedings of the National Academy of Sciences* **108**, 20935 (2011).
 - [18] Y. Liu, T. Liu, X.-Y. Yan, Q.-Y. Guo, H. Lei, Z. Huang, R. Zhang, Y. Wang, J. Wang, F. Liu, *et al.*, Expanding quasiperiodicity in soft matter: Supramolecular decagonal quasicrystals by binary giant molecule blends, *Proceedings of the National Academy of Sciences* **119**, e2115304119 (2022).
 - [19] E. Fayen, M. Impéror-Clerc, L. Filion, G. Foffi, and F. Smallenburg, Self-assembly of dodecagonal and octagonal quasicrystals in hard spheres on a plane, *Soft Matter* **19**, 2654 (2023).
 - [20] A. Plati, R. Maire, E. Fayen, F. Boulogne, F. Restagno, F. Smallenburg, and G. Foffi, Quasi-crystalline order in vibrating granular matter, *Nature Physics* **20**, 465 (2024).
 - [21] A. Gemeinhardt, M. Martinsons, and M. Schmiedeberg, Stabilizing quasicrystals composed of patchy colloids by narrowing the patch width, *Europhysics Letters* **126**, 38001 (2019).
 - [22] P. F. Damasceno, S. C. Glotzer, and M. Engel, Non-close-packed three-dimensional quasicrystals, *Journal of Physics: Condensed Matter* **29**, 234005 (2017).
 - [23] M. Dzugutov, Formation of a dodecagonal quasicrystalline phase in a simple monatomic liquid, *Physical review letters* **70**, 2924 (1993).
 - [24] G. Ungar and X. Zeng, Frank-kasper, quasicrystalline and related phases in liquid crystals, *Soft Matter* **1**, 95 (2005).
 - [25] E. G. Noya and J. P. Doye, A one-component patchy-particle icosahedral quasicrystal, arXiv preprint arXiv:2407.17212 (2024).
 - [26] M. Impéror-Clerc, A. Jagannathan, P. Kalugin, and J.-F. Sadoc, Square-triangle tilings: an infinite playground for soft matter, *Soft Matter* **17**, 9560 (2021).

- [27] M. Baake, R. Klitzing, and M. Schlottmann, Fractally shaped acceptance domains of quasiperiodic square-triangle tilings with dedecagonal symmetry, *Physica A: Statistical Mechanics and its Applications* **191**, 554 (1992).
- [28] J. Hermisson, C. Richard, and M. Baake, A guide to the symmetry structure of quasiperiodic tiling classes, *Journal de Physique I* **7**, 1003 (1997).
- [29] B. Grünbaum and G. C. Shephard, *Tilings and Patterns* (W.H. Freeman, New York, 1987).
- [30] M. Baake and U. Grimm, *Aperiodic Order: Volume 1, A Mathematical Invitation*, Vol. 1 (Cambridge University Press, Cambridge, 2013).
- [31] O. Perron, Zur theorie der matrices, *Mathematische Annalen* **64**, 248 (1907).
- [32] N. Pytheas Fogg, *Substitutions in Dynamics, Arithmetics and Combinatorics*, Lecture Notes in Mathematics, Vol. 1794 (Springer, Berlin, 2002).
- [33] A. L. D. Say-awen, D. Frettlöh, and M. L. A. N. De Las Peñas, On the frequency module of the hull of a primitive substitution tiling, *Acta Crystallographica Section A* **78**, 36 (2022).
- [34] D. Frettlöh, F. Gähler, and E. Harriss, Tilings encyclopedia, <https://tilings.math.uni-bielefeld.de>, accessed: 2025-01-01.